Deformation and Control Countermeasure of Surrounding Rocks for Water-Dripping Roadway Below a Contiguous Seam Goaf

Changqing Ma [1,2,*], Pu Wang [3,4,*], Lishuai Jiang [4] and Changsheng Wang [4,5]

[1] Department of Mechanical and Electronic Engineering, Shandong University of Science and Technology, Tai'an 271019, China

[2] Shanxi Coking Coal Refco Group Ltd., Huozhou 031400, China

[3] Department of Resources and Civil Engineering, Shandong University of Science and Technology, Tai'an 271019, China

[4] State Key Laboratory of Mining Disaster Prevention and Control, Shandong University of Science and Technology, Qingdao 266590, China; skwp0701@hotmail.com(L.J.); cswang0635@163.com (C.W.)

[5] Graduate School of Engineering, Nagasaki University, Nagasaki 852-8521, Japan

* Correspondence: changqing.ma@uconn.edu (C.M.); tianwailaike911@163.com (P.W.);
Tel.: +86-158-548-48872 (P.W.)

check for updates

Abstract: To solve the technical problem of supporting a water-dripping roadway below contiguous seams at the Tuanbai coal mine, the deformation law of surrounding rocks for the roadway was studied using Fast Lagrangian Analysis of Continua in Three Dimensions (FLAC3D) numerical simulation. Then, a mechanical model of water-dripping rock using a bolt support was established, and further, technical countermeasures to control the deformation of the roadway with a bolt and cable support are proposed. The results show that the erosion of the water dripping on the roadway was substantial and showed notable changes over time during roadway excavation and mining work. These effects caused the road to heave slightly, but it tended to be stable during roadway excavation. Moreover, the erosion of the roof and two ribs increased exponentially, and the floor heave increased with significant displacement oscillation during mining. The anchoring length of bolts and the rock weakening from water dripping had noticeable effects on the surrounding rocks of the roadway. The logical parameters of the bolt spacing and tightening force (the bolt line spacing was 0.7–0.9 m and the tightening force exceeded 40 kN) of the bolt supports were studied and optimized. Finally, a support scheme for water dripping on the roadway at the Tuanbai coal mine is proposed. The observation data regarding the deformation of the surrounding rocks, monitoring of bolt and cable stress, endoscopy results of roof failure, and roof bed separation monitoring were used to verify the reasonableness of the scheme and ensure the requirements for support were met. The study results can serve as a reference regarding the support for water dripping on a roadway under similar conditions.

Keywords: contiguous seams; water-dripping roadway; roadway deformation; bolt support

1. Introduction

Mining activities can change the structure and stress-state of coal and rocks, resulting in their deformation and destruction. Internal fractures of the rock masses develop and expand, eventually leading to the deformation of the roadway [1,2]. It is easy, then, to cause roof caving, rib spalling, and floor heaving or induce gas outburst and rock burst, possibly resulting in fatalities [3–7]. Several on-site photos of roadway instability are shown in Figure 1 [7].

Figure 1. Field photos after severe roadway damage.

Contiguous seams usually refer to coal seams having relatively small vertical distance and great shared effect when the coal seams are mined. The roof structure and the stress distribution of the lower coal seam in contiguous seams are affected significantly by upper coal mining, leading to the development of fractures that worsen gradually [8]. The main effect is that the strength of the surrounding rocks reduces, and the deformation of the roadway increases significantly [9]. When an aquifer occurs near the upper coal area, the water of the upper goaf affected by the aquifer failure can permeate into rock masses along the roof fractures of the lower coal seam. It weakens the strength of the surrounding rocks and aggravates the deformation failure of the roadway, thereby noticeably reducing the roadway stability further [10,11]. Hence, water dripping below a contiguous seam onto the roadway below results in the need to strengthen the roadway.

Bolt support, which has been widely used in roadway support, can form a stable bearing structure with the interaction between the bolt and the rock in the corresponding zone. It can change the stress state of surrounding rocks and increase confining pressure, thereby improving the bearing capacity of the surrounding rocks and restraining the development of the fractured zone [12]. Many studies show that bolt support can markedly enhance the compressive strength of the surrounding rocks of a roadway [13].

Many studies have been conducted regarding the evolution of mining-induced stress and deformation failure of the surrounding rocks for a roadway below a contiguous seam. Zhao [14] and Yang et al. [15] studied the evolution laws of deformation failure and mining-induced stress of the surrounding rocks for roadways, with or without water immersion during roadway excavation, by numerical simulation. Yang [16] and Wu [17] studied roadway stability below a goaf of a contiguous seam and found that the roadway was supported easily with a large coal pillar from the upper coal seam and a large distance away from the upper coal seam. Dunning et al. [18] showed water could change the structure and composition of rocks, resulting in the reduction of strength, cohesion, and the friction coefficient. Hawkins and McConnell [19] carried out uniaxial compression strength tests of 35 kinds of sandstone under dry and saturated conditions and found that water pressure had little effect on the rock strength. Chugh and Missavage [20] showed the uniaxial compression strength of rock specimens reduced significantly under the conditions of water and 100% humidity. Ren [21] studied the displacement field, stress field, and seepage field affected by water, utilizing several methods, such as numerical simulation, theoretical analysis, and field observation; moreover, Ren showed that the support of a composite structure with pre-stressed steel bolts and rocks can achieve a better active securing effect. Zhang et al. [22] suggested some support schemes based on the differences in the distance between roof rock and coal seam to be conscious of safe roadway excavation and mining work.

Currently, regarding the theories for and experiences in the control of roof strata with single coal seam mining or long-distance coal seam mining, considerable studies have been conducted; however, they cannot explain adequately the strata pressure appearance and mechanisms underlying the conditions of contiguous seam mining. Contiguous seam mining, stress, and deformation of the

surrounding rocks for a roadway are often studied, but the stability of the surrounding rocks and the corresponding support scheme for the roadway affected by dripping water are rarely discussed. Hence, in view of the geological and mining conditions (dripping water and contiguous seams), such as the deformation of the surrounding rocks by the water dripping on a roadway below a contiguous seam goaf, the mechanical model of the surrounding rocks with bolt support is established here. In this paper, the effect of bolt anchorage length and water-dripping erosion on rock strength is studied. The combined support scheme of bolt and cable is suggested, and two important technical parameters of bolt support (bolt line spacing and tightening force) are examined in detail. Furthermore, feasible measures for support to control this geological condition are suggested. The study results not only can provide a theoretical basis and technical guidance for solving the issues of support and control of the surrounding rocks for water dripping on a roadway below a contiguous seam goaf, but also can serve as a reference for the application of roadway support under similar geological conditions; thus, they are worthy of further research.

2. Numerical Analysis of Deformation for a Water-Dripping Roadway

2.1. Engineering Overviews of Tuanbai Coal Mine

Coal seam no. 11 of the Tuanbai coal mine in the Shanxi province is below coal seam no. 10. The vertical distance between the two seams is 40 m, and they are contiguous seams. Due to the mining activities and an aquifer fracture, a lot of water accumulates in the goaf after the no. 10 coal seam mining exit, leading to floor strata fracture and conspicuously affecting the roof stability of the working area in the no. 11 coal seam.

Panel 11-101, which is the testing area for the no. 11 coal seam, is below the goaf of the no. 10 coal seam and is 5.4 m away from the upper goaf. The mining depth and height of Panel 11-101 are 300–357 m and 3.1–3.3 m, respectively. Regarding the geologic column shown in Figure 2, hard siltstone is between the two coal seams and is not deformed, expanded or affected by water.
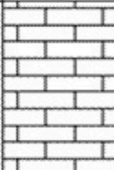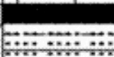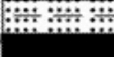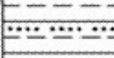
Litho-logy	Thickness /m	Histog-ram
Lime stone	9.2	
No.9 coal	1.0	
Silt stone	2.3	
No.10 coal	2.7	
Silt stone	5.4	
No.11 coal	3.7	
Mud-stone	8.5	

Figure 2. Geologic column of Panel 11-101.

2.2. Numerical Model Establishment

The numerical simulation methods, which are widely used in mining engineering, can be used to effectively solve complex engineering problems [23]. The Fast Lagrangian Analysis of Continua in Three Dimensions (FLAC3D) software can simulate the stress field and deformation field of a roadway with complex conditions during the process of excavation and has achieved many research results. FLAC3D was developed by the ITASCA consulting group of the United States of America (U.S.A.) and has become one of the most important numerical methods for rock and soil mechanics calculation. It can simulate the mechanical properties of three-dimensional soil, rock mass, and other geological materials, especially the plastic rheological properties when they reach their yield limit. It is also suitable for the analysis of progressive failure and large deformation. Moreover, it consists of 11 constitutive models of elastoplastic materials, including static, dynamic, creep, seepage, and temperature calculation models. Hence, it is widely used in many fields like slope stability evaluation, support design and evaluation, tunnel engineering, and mine engineering [24]. Therefore, it can meet the needs of this study. This software provides an idea and method for evaluating the stability and the optimization of a support system for the roadway [25]. Based on the geological conditions of Panel 11-101 of the Tuanbai coal mine, a FLAC3D numerical model was established concerning the goaf from the upper coal seam and a roadway for the lower coal seam experiencing a water-dripping condition.

To meet the requirements of the study in this paper, the thicknesses of the roof–floor strata of Panel 11-101 were adjusted. Considering the boundary effect, a simulation model with dimensions of 200 m (length) × 50 m (width) × 100 m (height) was established, as shown in Figure 3. Herein, following the upper coal seam of the no. 10 mines, the size of the goaf is 150 m (dip length) × 50 m (strike width) × 100 m (height); the size of the roadway in the lower coal seam, with a mining depth of 350 m and a distance from the upper coal seam of 40 m, is 4.3 m (width) × 2.7 m (height).
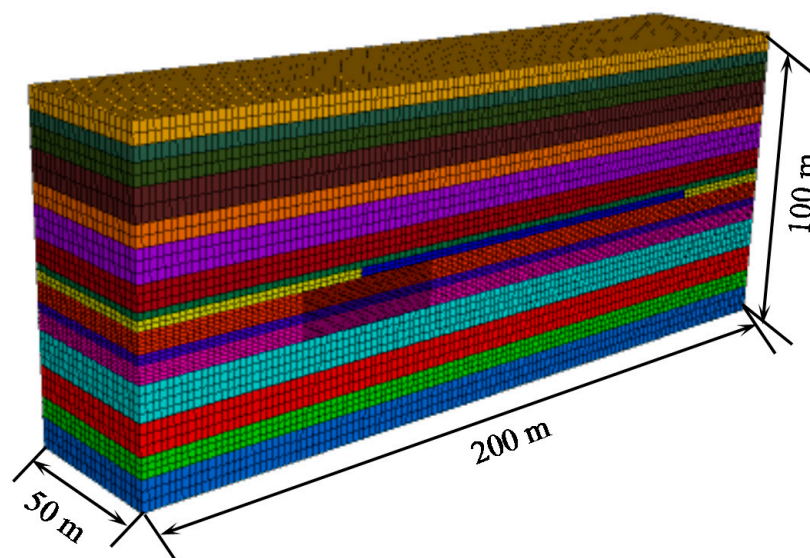

Figure 3. Numerical calculation model.

The mechanical properties assigned to the model were conventionally derived from laboratory testing programs [26]. Table 1 lists the parameters of the main rocks derived from the geological report for Panel 11-101. The Mohr–Coulomb model was used to simulate the failure of coal and rock masses. Considering the water accumulation in the goaf of the upper coal seam and its weakening effect on the rock strength, the double yield model was used to simulate the goaf of the upper coal seam.

Table 1. Mechanical properties of rock masses.

Lithology	Bulk/GP	Shear/GPa	Cohesive/MPa	Internal Angle/°	Tensile Strength/MPa
Coal seam	0.92	0.83	1.68	20	1.340
Limestone	22.6	11.1	4.72	32	7
Siltstone	6.11	4.84	2.30	30	4.47
Fine sandstone	5.87	3.38	3.26	28	3.19
Aluminous mudstone	3.06	1.89	1.80	26	3.89
Mudstone	2.17	1.21	1.30	25	2.78

The full displacement constraint boundary, in this numerical model, was used for the bottom, while the horizontal displacement constraint and uncontrolled vertical displacement were used at the left and right sides; moreover, the top boundary was unstructured. According to the calculation method of reference written by Wang et al. [7], the failed simulation of the overlying strata in this model was presumed to be the vertical stress of 7.50 MPa acting on the top boundary. Based on the geological report on Panel 11-101, the value of the horizontal stress applied to the two sides of the model with the trapezoidal distribution was half of the value of the vertical stress.

2.3. Numerical Scheme

(1)　Stage of Roadway Excavation

The roadway in the no. 11 coal seam was excavated after the upper working phase of the no. 10 mine exit, and the total excavation length was set to be 200 m. A section of roadway at the starting position of the excavation and an arrangement of four monitoring points were selected—located in the roof, two ribs, and the floor—to monitor the deformation of the roadway. Hence, during the roadway excavation, the distance between the heading face and the surveyed section rose gradually.

(2)　Stage of Working Face Mining

Panel 11-101 was mined after the completion of the roadway excavation. A section of roadway 50 m from the opening was selected, and four monitoring points similar to those in the previous step were arranged around the stage of the roadway excavation to monitor the deformation of the roadway affected by the mining activities. Thus, during mining, the distance between the work area and the monitoring section in the survey range decreased gradually.

2.4. Simulation Results of Roadway Deformation

Due to the roadway excavation or the mining phase, the roadway became deformed. Hence, the roadway deformation showed a noteworthy effect during the roadway excavation and the mining phases. Moreover, it presented significant stage characteristics, as shown in Figure 4.

Figure 4a,b show that the deformation variations of the roof subsidence and the two ribs were similar. The notably affected zone of the roadway mainly occurred at the initial stage of the roadway excavation and the stage during mining. The deformation variations rose sharply at the initial stage of roadway excavation, with the maximum values at 0.21 m and 0.11 m, represented by Stage I. Continuing with the roadway excavation, the subsidence values had little change and the subsidence rate was smaller (Stage II). Following the commencement of mining during the working phase, the deformations increase notably (Stage III); however, the subsidence rose with ladder-shape when the monitoring point was more distant from the work area, and then it was affected sharply by significant abutment stress.
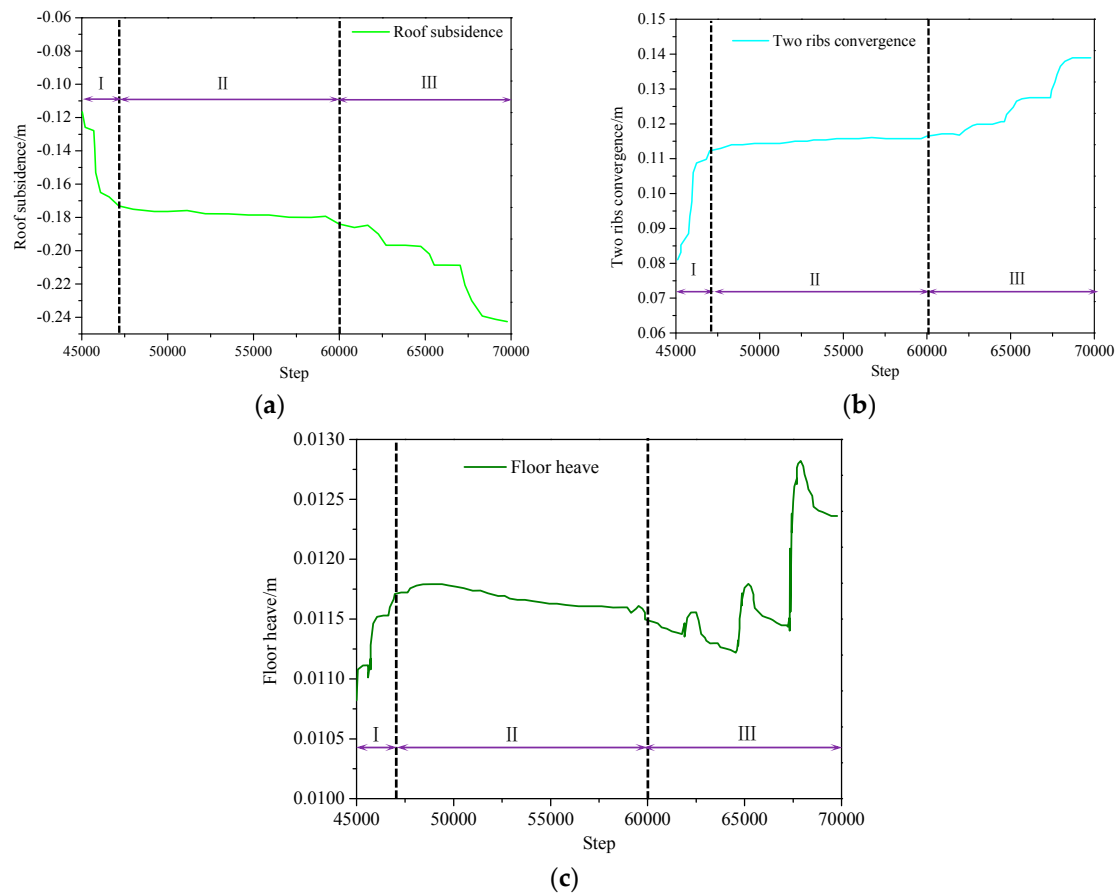
Figure 4. Variation curve of roadway deformation. (**a**) Roof subsidence; (**b**) Two ribs' convergence; (**c**) Floor heave deformation.

Figure 4c displays that the deformation variation of the floor heave found in Stage I was similar to that of the roof and two ribs' distortion. However, the variations of Stage II and Stage III were different, when comparing the warp of the floor heave, roof, and two ribs. During roadway excavation within Stage II (see Figure 4c), the deformation lessened slightly due to abutment stress transfers and reduction. During the mining phase of Stage III (see Figure 4c), the floor heave increased with significant displacement oscillation, and then dropped sharply when the surveyed section was already into the goaf of Panel 11-101.

Thus, it can be concluded that in the initial stage of the roadway excavation (corresponding to Stage I in Figure 4), the deformation of the roadway (roof subsidence, two ribs converging, and floor heave, for example) rose sharply and the increase rate was large. During the middle and late stages of the roadway excavation (Stage II in Figure 4), the deformation varied slightly; herein, the deformation of the roof and two ribs increased, while that of floor heave decreased. Stage III in Figure 4, shows that the deformation rose again as a whole when affected by mining activities; however, the deformation of the roof and two ribs showed ladder-shaped growth, while that of the floor heave presented substantial displacement oscillation.

3. Mechanical Analysis of Water-Dripping Rock with Bolt Support

Garnered from the simulation analysis in Section 2, the roadway of Panel 11-101 had large deformations and could not be used normally; hence, bolt support was used for roadway maintenance. Bolt support can control the deformation and the failure of the surrounding rocks and maintain the integrity to the maximum in the anchor zone, thereby enhancing the strength and stability of the surrounding rocks [27,28].

3.1. Mechanical Model of Water-Dripping Rock with Bolt Support

Figure 5 shows a mechanical model of fractured rock with a bolt support. The maximum principal stress σ_1 and minimum principal stress σ_3 wrought on the rock, and the normal stress and shear stress that take effect on the fracture plane (Plane AB), are set to σ and τ in this model. When a bolt support goes through Plane AB, the relationship between the shear stress and shear displacement can be expressed by Equation (1) as follows [29]:

$$\tau = Ku \tag{1}$$

where τ is the shear stress, MPa; u is the shear displacement, m; and K is the interface stiffness factor of the fracture Plane AB without water dripping obtained by a rock test.
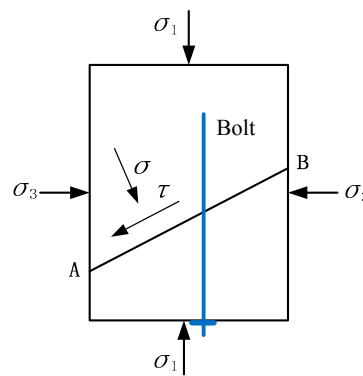

Figure 5. Mechanical model of fracture rock with bolt support.

When the rocks encounter water, their strength weakens. Hence, erosion factors of a rock fracture are marked as D^m (with water dripping) are defined by Equation (2) as follows:

$$D^m = \frac{K - K'}{K} \tag{2}$$

where K' is the interface stiffness factor of the fracture plane with water dripping. Herein, D^m is in the range of 0–1, and $D^m = 0$ means that the rock is affected by water, while $D^m = 1$ indicates that the rock fractures completely. Thus, the relationship between shear stress and shear displacement with water-dripping can be expressed by Equation (3).

$$\tau = (1 - D^m)Ku \tag{3}$$

When the shear stress of the interface between the bolt—coated with epoxy resin to prevent corrosion—and the surrounding rock is less than its shear strength, the interface is in a completely elastic state without relative displacement. Therefore, the bolt and the surrounding rock need to meet the deformation coordination conditions. Figure 6 shows the stress analysis of the bolt.

According to Hooke's law, the relationship between the displacement of the bolt $u(z)$ and the axial stress of the bolt $P(z)$ at the depth of z can be expressed by Equation (4) as follows:

$$\frac{du(z)}{dz} = -\frac{4P(z)}{\pi D^2 E_a} \tag{4}$$

where E_a is the equivalent elastic modulus of the bolt-coating, $E_a = \frac{E_m(D^2 - d^2) + E_b d^2}{D^2}$, MPa; E_m and E_b are elastic modulus of the bolt coating and bolt, MPa; D and d are the diameters of the bolt coating and bolt, respectively, m; and L_b is the anchorage length, m.
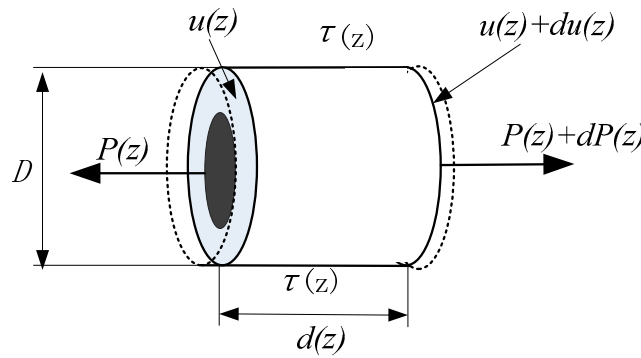
Figure 6. Stress analysis of bolt-coating body.

Based on the static equilibrium of a unit on the bolt coating, the shear stress of the bolt $\tau(z)$ with the depth of z can be expressed by Equation (5).

$$\frac{dP(z)}{dz} = -\pi D\tau(z) \tag{5}$$

According to the boundary conditions of the bolt coating in Equation (6), the shear stress of the bolt-$\tau(z)$ with the depth of z is obtained via Equation (7) as follows:

$$\begin{cases} \left. \dfrac{E_a D^2 \pi du(z)}{4dz} \right|_{z=0} = -P \\[4mm] \left. \dfrac{E_a D^2 \pi du(z)}{4dz} \right|_{z=L_b} = 0 \end{cases} \tag{6}$$

$$\tau(z) = \frac{\lambda \cosh[\lambda(L_b - z)]}{\pi D \sinh(\lambda L_b)} P \tag{7}$$

where λ is a constant, $\lambda = \sqrt{\frac{4(1-D^m)K_1}{DE_a}}$

When the interface between the bolt linkage is in elastoplasticity, the shear stress of the bolt truss at $z = 0$ reaches its ultimate shear strength. Thus, the ultimate pulling force of the bolt fixture P_u is obtained as shown in Equation (8).

$$P_u = \frac{\pi D(1 - D^m)\tau \tanh(\lambda L_b)}{\lambda} \tag{8}$$

Thus, from Equation (8), the ultimate pulling force of the bolt P_u had a close relation to the anchoring length L_b, water-dripping erosion factors D^m, and other factors.

When the fractured rock supported by a bolt slipped along the fracture Plane AB, the upper part of the rock above the fracture plane was selected and analyzed. Figure 7 shows the mechanical analysis for the slipping of the fractured rock supported by a bolt.

Regarding the bolt, the shear stress along the fracture plane affected by the bolt was broken down into the shear stress τ_N and the tensile stress τ_P, as expressed in Equation (9).

$$\begin{cases} \tau_N = (\tau - c - \sigma \tan \varphi) \cos \alpha \\ \tau_P = (\tau - c - \sigma \tan \varphi) \sin \alpha \end{cases} \tag{9}$$

where c is the cohesive of the fracture Plane AB, measured in MPa; and φ is the internal angle of the fracture plane, measured in degrees.
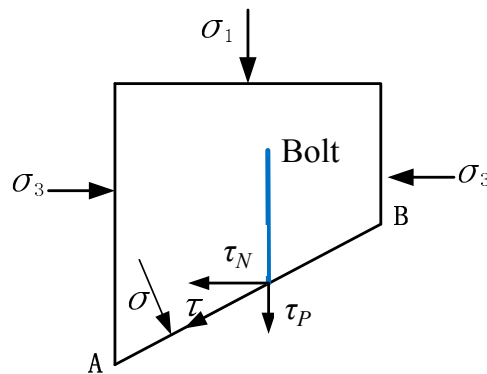
Figure 7. Mechanical model with the slipping of fracture rock supported by a bolt.

The stress of the fracture Plane AB, if Plane AB bears the osmotic stress p' affected by dripping water, can be obtained as shown in Equation (10).

$$\begin{cases} \sigma = \frac{1}{2}(\sigma_1 + \sigma_3) + \frac{1}{2}(\sigma_1 - \sigma_3)\cos 2\alpha - p\prime \\ \tau = \frac{1}{2}(\sigma_1 - \sigma_3)\sin 2\alpha \end{cases} \tag{10}$$

Concerning the fracture rock supported by the bolt, there are two failure modes when the bolt fails, for the most part. One is shear failure along the fracture Plane AB, and the other is the slipping failure between the bolt and the rock.

Assuming the shear strength of the bolt body is τ_b, the bolt will be in the limited equilibrium state of shear failure with $\tau_N = \tau_b$. Hence, Equation (11) can be obtained as follows:

$$\sigma_1 = \sigma_3 + \frac{2(c + \sigma_3 \tan \varphi - p' \tan \varphi + \tau_b/\cos \alpha)}{\sin 2\alpha - \cos 2\alpha \tan \varphi - \tan \varphi} \tag{11}$$

The bolt fixture and rock mass will be in the limited equilibrium state of slipping failure with $\tau_P \frac{\pi D^2}{4} = P_u$ if the anchorage interface is in a complete elastic state. Hence, Equation (12) can be obtained as follows:

$$\sigma_1 = \sigma_3 + \frac{2[c + \sigma_3 \tan \varphi - p' \tan \varphi + 4(1 - D^m)\tau_b \tanh(\lambda L_b)/D\lambda \sin \alpha]}{\sin 2\alpha - \cos 2\alpha \tan \varphi - \tan \varphi} \tag{12}$$

Thus, from the previous analysis, the strength of the fracture rock supported by the bolt drops due to deterioration by dripping water and the reduction of the anchoring bolt length.

3.2. Effect of Anchorage Length and Water-Dripping Erosion Factor on Rock Strength

3.2.1. Effect of Anchorage Length on Rock Strength

To study the effect of anchorage length on rock strength, different anchorage lengths of a bolt, such as 0.1 m, 0.2 m, 0.5 m, 1.0 m, and 2.0 m, were examined. Equations (11) and (12) show that the main parameters included the following: $\sigma_3 = 2$ MPa, $c = 0.5$ MPa, $\varphi = 22°$, $D = 0.03$ m, $p' = 0.5$ MPa, $\tau_b = 0.6$ MPa, $D^m = 0$, and $\lambda = 2.83$. Hence, the relationship between the maximum principal stress σ_1 and the dip angle of the fracture Plane AB with the different anchorage lengths is shown in Figure 8.
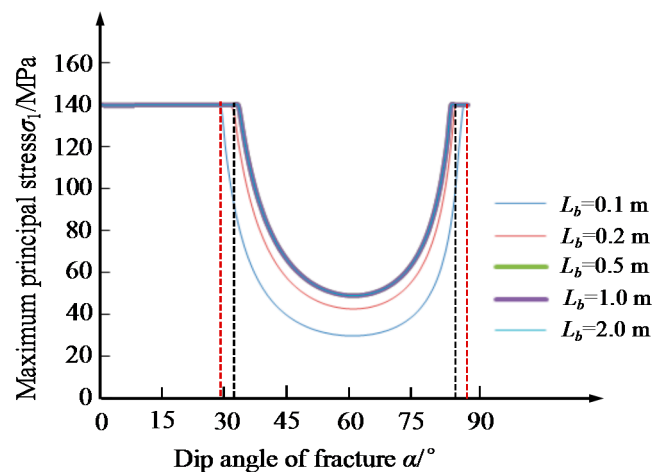
Figure 8. Effect of different anchorage lengths on rock strength.

In Figure 8, the variation curves of rock strength with different anchorage lengths are similar. However, the dip angle of the rock slipping along the failure face AB with different anchorage lengths is different, which indicates that the effects of anchorage lengths on rock strength are different.

The maximum principal stress increased significantly with $L_b \leq 0.5$ m, while having little change within 0.5 m < $L_b \leq 2.0$ m. Moreover, the affected range of the dip angle for the rock slipping along the failure Plane AB decreased with $L_b \leq 0.5$ m, while it had little change within 0.5 m < $L_b \leq 2.0$ m, as shown in Table 2. When L_b = 0.1 m, the rock failed along the fracture Plane AB within $29° \leq \alpha \leq 86°$, and the minimum value was 29.7 MPa, for example; when L_b = 0.5 m, the rock failed along the fracture plane within $34° \leq \alpha \leq 83°$, and the minimum value increased to 48.9 MPa.

Table 2. Dip angle of rock slipping along the failure face AB with different anchorage lengths.

Anchorage Length L_b/m	Dip Angle of Rock Slipping along the Failure Face α/°
0.1	$29° \leq \alpha \leq 86°$
0.2	$32° \leq \alpha \leq 84°$
0.5	$34° \leq \alpha \leq 83°$
1	$34° \leq \alpha \leq 83°$
2	$34° \leq \alpha \leq 83°$

Therefore, it can be concluded that there is an optimal value for the anchor length's capacity to support the roadway. When the anchor length is less than its optimal value, the support effect rises noticeably as the anchor length increases, while it is not obvious once the anchor length exceeds the optimal value.

3.2.2. Effect of Water-Dripping Erosion Factor on Rock Strength

To study the effect of the water-dripping erosion factor on rock strength, different water-dripping erosion factors, such as 0, 0.3, 0.6, and 0.9, were studied. Similar to the parameters in Section 3.2.1, some boundaries were added and adjusted, such as K = 0.6 GPa/m and E_a = 10 GPa. The relationship between the maximum principal stress σ_1 and the water-dripping erosion factor is shown in Figure 9.

Figure 9 shows the variation curves of rock strength with different water-dripping erosion factors are similar; the weakening effect on the rock strength and the affected range of the dip angle for rock slipping along the failure face AB increased markedly as the erosion factors rose. When D^m = 0, the rock failed along the fracture Plane AB within $34° \leq \alpha \leq 84°$ (as shown in Table 3) and the minimum value was 49 MPa, for example; when D^m = 0.3, the rock failed along the fracture Plane AB within $32° \leq \alpha \leq 84°$, and the minimum value fell to 41.9 MPa; when D^m = 0.6, the rock failed along the

fracture Plane AB within $30° \leq \alpha \leq 86°$, and the minimum value was 32.9 MPa; when $D^m = 0.9$, the rock failed along the fracture Plane AB within $27° \leq \alpha \leq 87°$, and the minimum value fell to 19 MPa. The rock strength decreased from 41.9 MPa to 19 MPa as the erosion factor rose, making the weakening effect obvious.

Hence, it can be concluded that the rock strength can be enhanced by increasing the anchor length or by decreasing the water-dripping erosion factor, thereby enhancing the support for the roadway.

Table 3. Dip angle of rock slipping along the failure face with different water-dripping erosion factors.

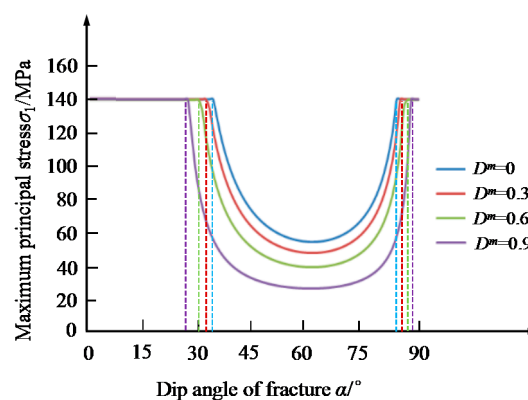| Water-Dripping Erosion Factors D^m	Dip Angle of Rock Slipping along the Failure Face $\alpha/°$
0	$34° \leq \alpha \leq 84°$
0.3	$32° \leq \alpha \leq 84°$
0.6	$30° \leq \alpha \leq 86°$
0.9	$27° \leq \alpha \leq 87°$

Figure 9. Effect of different water-dripping erosion factors on rock strength.

4. Numerical Analysis of Deformation of a Water-Dripping Roadway with Bolt Support

4.1. Results of Numerical Simulation

Deformation of a roadway with water dripping onto it is sizeable (see Section 2); however, bolt support can effectively restrain deformation (see Section 3). Hence, based on the numerical simulation used in Section 2, an alternate model of a roadway with bolt support is established and used to compare with the model without bolt support. Regarding the model with bolt support, the support parameters mainly included a bolt diameter of 18 mm, bolt length of 2200 mm, and bolt spacing of 900 × 900 mm.

To study the effect of the bolt support on the roadway, the index of deformation and failure of roadway, such as roof subsidence, maximum principal stress, and plasticity zone, were studied and discussed. Figures 10–12 depict the nephogram regarding these three indices of roadway, with or without bolt support.

Figures 10–12 display that the peak values of the three indices—roof subsidence, maximum principal stress, and plasticity zone distribution—without bolt support were larger than those with bolt support. The peak values of roof subsidence with or without bolt support were 48.37 mm and 60.63 mm, respectively, which reduced the amount of subsidence by 20% with bolt support, for example; the maximum principal stress without bolt support was 0.062 MPa of tensile stress, while that with bolt support was −0.0063 MPa of compressive stress. Moreover, the range of the plasticity zone without bolt support was substantial, mainly having tensile and shear failures, whereas that with bolt support decreased noticeably with mainly shear failure. The results indicate that bolt support can significantly reduce the roof subsidence and plasticity range of a roadway; meanwhile, it greatly drops the maximum principal stress and changes the stress state from tensile stress to compressive stress,

which can enhance the rock strength markedly. Thus, bolt support has a good effect on controlling the deformation and failure of a roadway, thereby maintaining its stability.
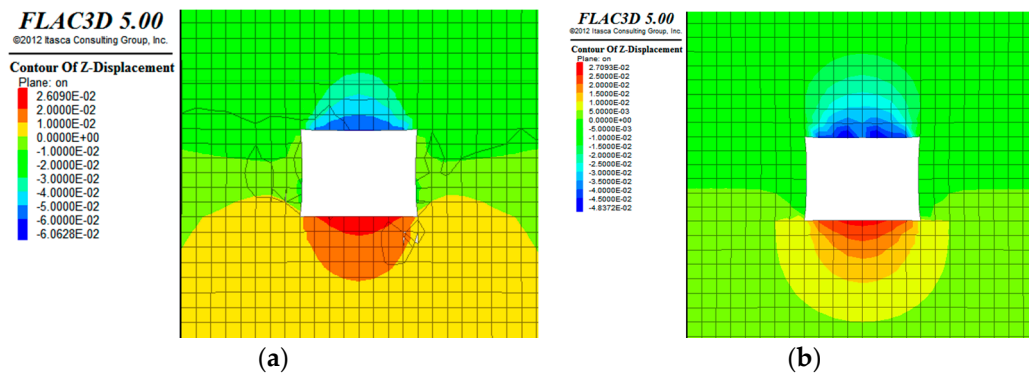

Figure 10. Nephogram of the roof subsidence with or without bolt support. (**a**) Without bolt support; (**b**) With bolt support.
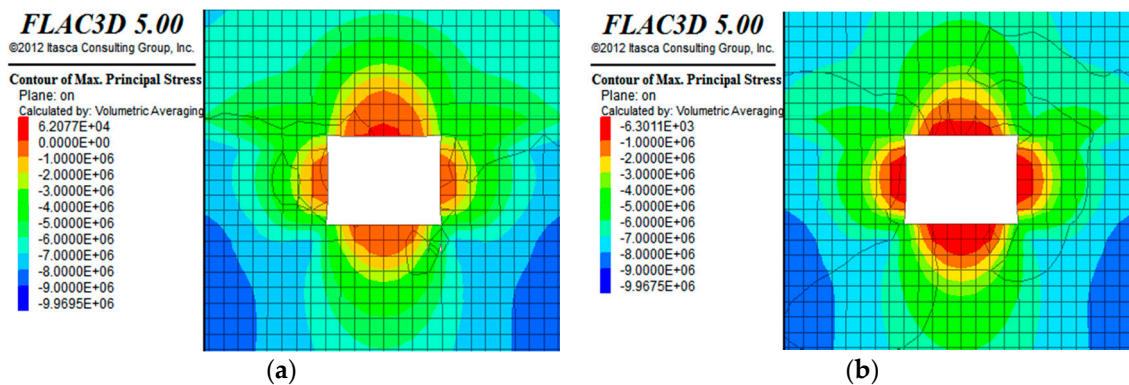

Figure 11. Nephogram of the maximum principal stress with or without bolt support. (**a**) Without bolt support; (**b**) With bolt support.
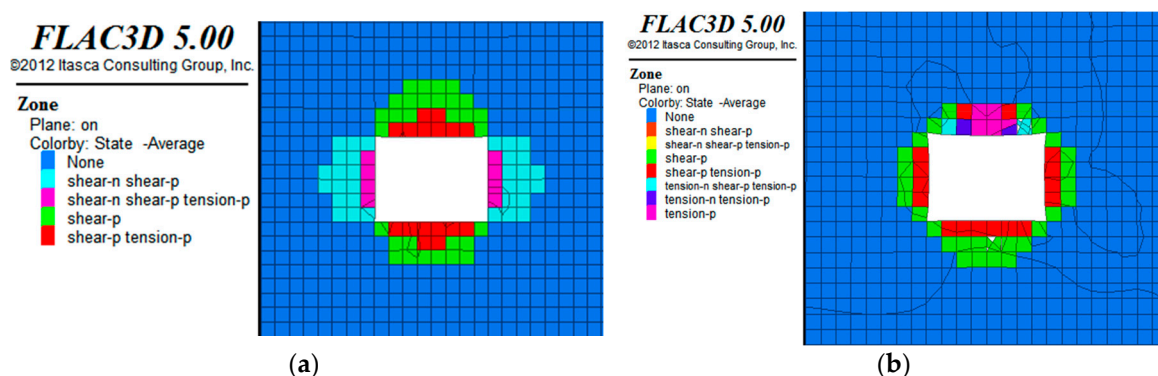

Figure 12. Nephogram of the plastic zone with or without bolt support. (**a**) Without bolt support; (**b**) With bolt support.

4.2. Effect of Bolt Parameters on Roadway Stability

According to the reference written by Kang et al. (2008), the line space and tightening force of bolts are the important technical parameters of bolt support for the roadway. The line spacing of bolts directly determines the range of the compressive stress of the surrounding rocks. The effect of different

line spacing and different tightening force on the stability of a roadway was studied using the control variable method, which only changed line spacing or tightening force.

4.2.1. Effect of Line Space of Bolt on Roadway Stability

To study the effect of the spacing of the bolts on the roadway stability, the roof subsidence and the plasticity zone are displayed in Figures 13 and 14. Herein, the tightening force of a bolt was set to 40 kN and remained unchanged, and the different spacing of the bolts, such as 0.6 m, 0.7 m, 0.8 m, 0.9 m and 1.0 m, were the variable.
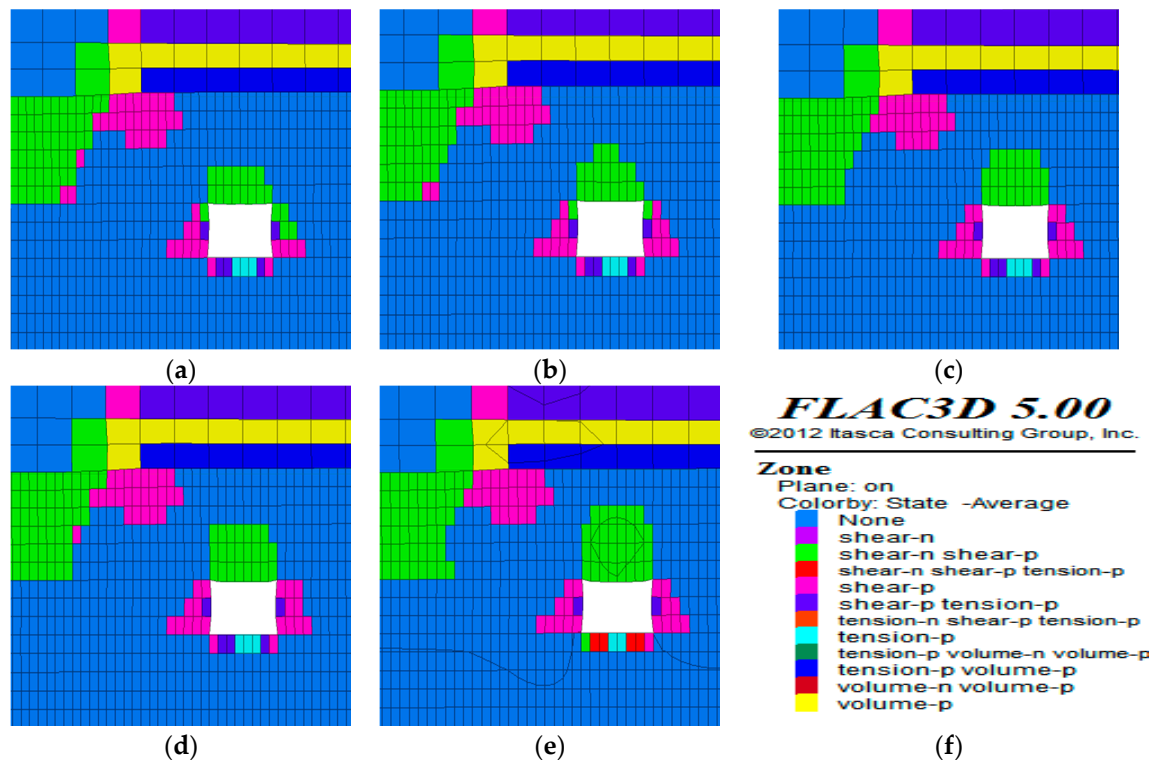
Figure 13. Range of the plasticity zone of the roadway with different line spacing of the bolts. (**a**) 0.6 m; (**b**) 0.7 m; (**c**) 0.8 m; (**d**) 0.9 m; (**e**) 1.0 m; (**f**) Rock failure state.
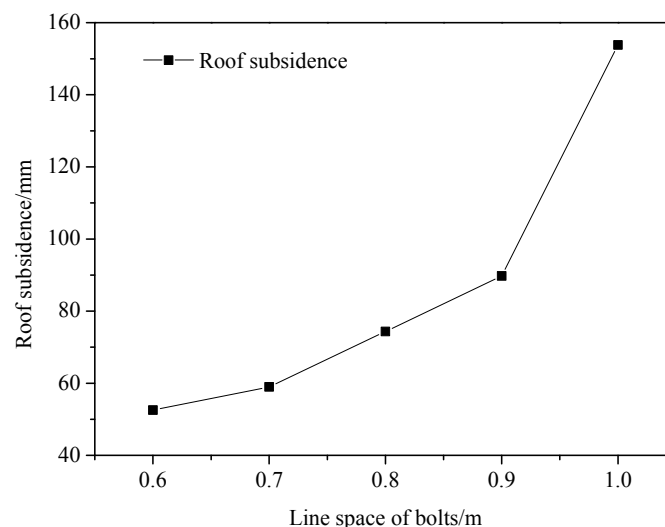
Figure 14. Variation of the roof subsidence for the roadway with different line spacing of bolts.

Figures 13 and 14, with the spacing of the bolts increasing from 0.6 m to 1.0 m, show the range of the plasticity zone, while the roof subsidence of the roof rock increased, indicating that the support effect of the bolt weakened. However, the two parameters increased gradually as the spacing escalated from 0.6 m to 0.9 m, with a significant rise in the spacing of 1.0 m. Herein, the roof subsidence rose slightly from 52.56 mm to 89.74 mm as the line spacing increased from 0.6 m to 0.9 m, and it markedly rose to 153.85 mm with the spacing of 1.0 m, with an increase of 63% compared to the spacing at 0.9 m. Thus, the closer spacing/greater frequency of the bolts has better support for the roadway; however, too little space between the bolts will significantly raise the cost.

Thus, from the analysis of the roof subsidence and plasticity range, the spacing of the bolts should be selected between 0.7 m and 0.9 m, according to this simulation.

4.2.2. Effect of Tightening Force of Bolt on Roadway Stability

To study the effect of the tightening force of the bolts on roadway stability, the roof subsidence and the plasticity zone are displayed in Figures 15 and 16. Herein, the spacing of bolts was set to 0.9 m and remained unchanged, and the different tightening force of the bolts, such as 20 kN, 40 kN, 60 kN and 80 kN, were the variable.

Figures 15 and 16, with the tightening force of the bolts increasing from 20 kN to 80 kN, show the range of the plasticity zone and the subsidence of the roof rock, which indicate that the bolt enhances the support effect. However, the two parameters dropped gradually with the tightening force of 20 kN and 40 kN, while they decreased noticeably with the tightening force of 60 kN and 80 kN. Herein, the roof subsidence dropped slightly from 95.15 mm (assuming the tightening force was 20 kN) to 88.98 mm (if the tightening force was 40 kN), and it markedly decreased to 55.28 mm with the tightening force of 80 kN. Hence, the stronger tightening force, exceeding 40 kN, had better support for the roadway.

Thus, the line spacing and the tightening force of the bolts have significant effect on the roadway support. Moreover, it can be concluded that the reasonable parameters of bolts with the spacing of 0.7–0.9 m and a tightening force exceeding 40 kN for roadway support are more effective.
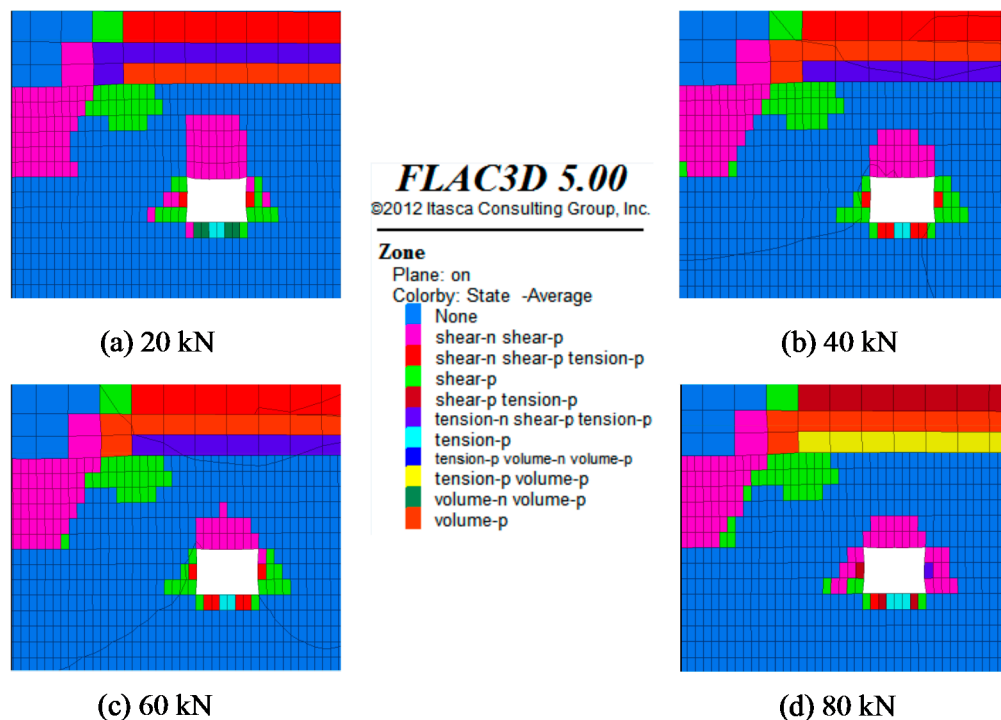

(a) 20 kN　　　　(b) 40 kN

(c) 60 kN　　　　(d) 80 kN

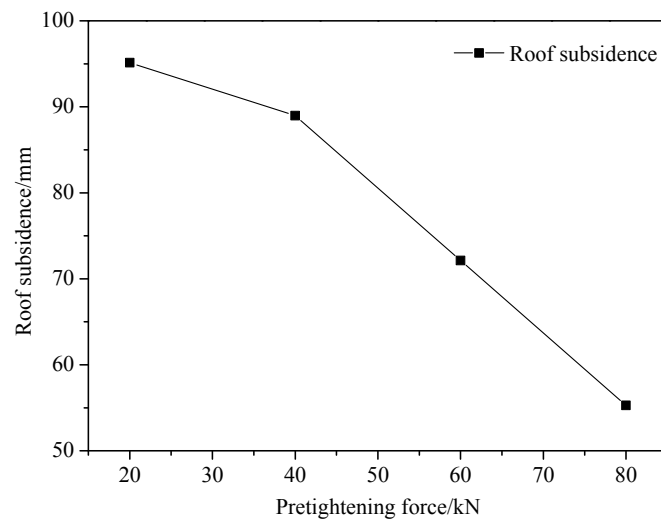**Figure 15.** Range of the plasticity zone of the roadway with different tightening forces.

Figure 16. Variation of the roof subsidence for the roadway with different tightening forces.

5. Field Observations About Support Effect of Roadway with Dripping Water

5.1. Support Scheme

According to the geological report for Panel 11-101, a scheme of bolt and cable support for the roadway was carried out, as shown in Figure 17. Based on the previous studies, the mechanism of a cable support was similar to that of a bolt support; however, the support effect of the cable was more obvious than that of the bolt support. Hence, the bolt and cable support for the roadway could better control the deformation of the surrounding rocks [6,13].
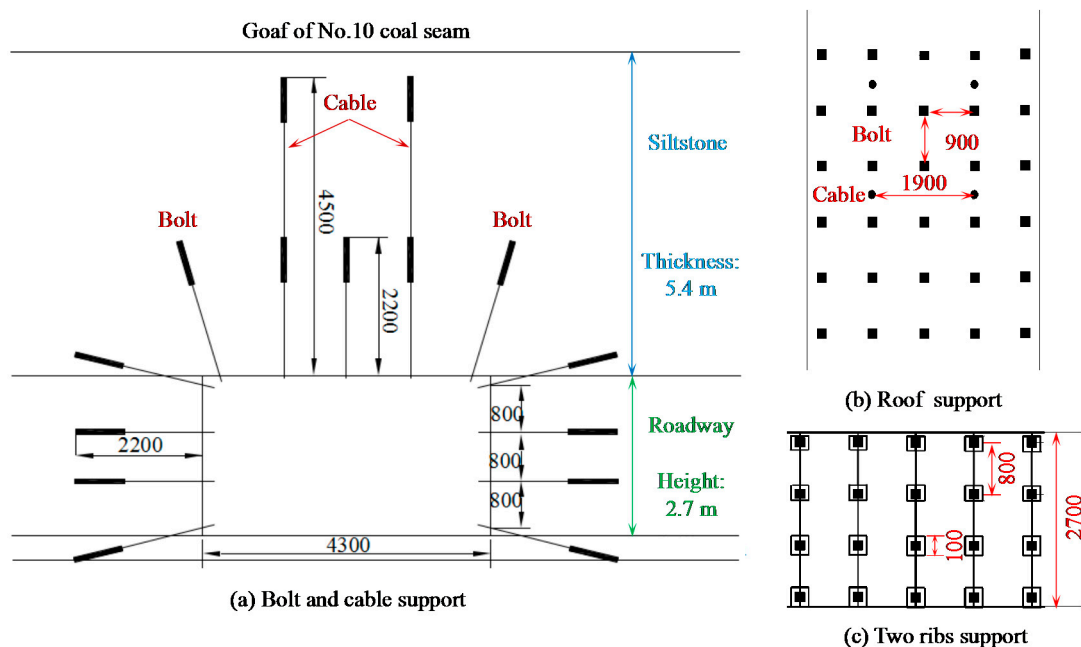

Figure 17. Scheme of bolt and cable support.

It can be divided into bolt support and cable support in this analysis, and the main parameters are as follows:

(1)   Bolt Support System. The system used a high strength bolt made of screw steel, measuring Φ18 × 2200 mm, and used a tightening force exceeding 40 kN. The anchoring agent marked as FSCK2340 had waterproof resin properties. The line and row spacing of the bolts were 800 mm and 900 mm, respectively.

(2)   Cable Support System. The system used a cage-type cable, measuring Φ 17.78 × 4500 mm, with a tray size of 100 × 100 × 10 mm. The anchoring agent marked as FSCK2340 × 4 was a waterproof resin.

5.2. Analysis of Field Observation

A section of the roadway was selected as the starting position for the excavation and the assembly of four monitoring points located in the roof, two ribs, and floor to monitor the deformation of the roadway. Moreover, the roof development and bolt and cable forces are discussed. The observation data are shown in Figures 18–20.

5.2.1. Observation with Roadway Excavating

(1)   Deformation Monitoring of Roadway

Table 4 and Figure 18 show that, with roadway excavation, the variation of the roadway deformation, such as roof subsidence, two ribs' convergence, and floor heave, had similar growth tendencies. When the excavating distance exceeded 100 m, the roof subsidence and two ribs' convergence tended to be stable, while the floor heave also tended to be stable when the mining distance exceeded 200 m. Moreover, the roof subsidence and two ribs' convergence had small peak values, which indicated that the bolt and cable support effectively restrained the deformation of the roadway with good support; however, the floor heave was relatively large due to the significant effect of the dripping water.

Table 4. Deformation variation of the roadway with roadway excavating.

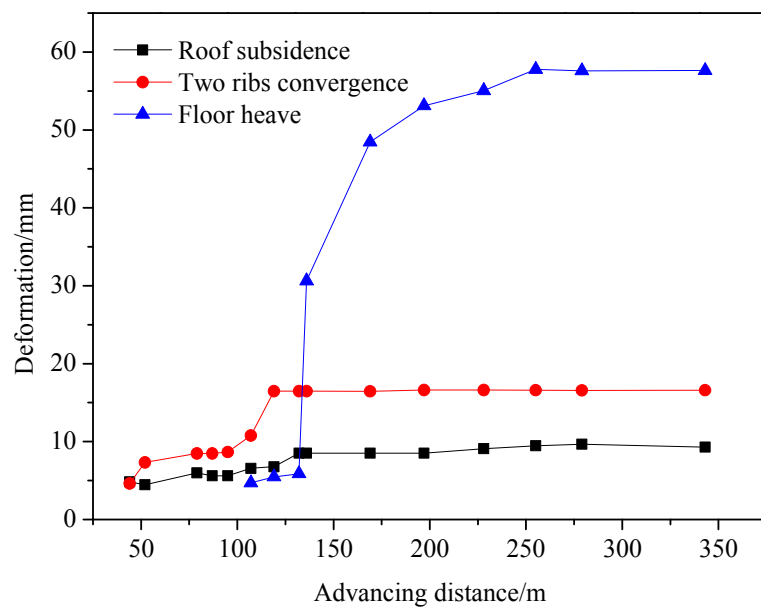| Excavating Distance/m	Roof Subsidence/mm	Floor Heave/mm	Two Ribs' Convergence/mm
1.5	0		0
9	0		3
40.5	1		4
49.5	1		4
57	1		4
72.5	2	0	6
86	2	1	16
101.5	4	1	16
105.3	4	28	16
143	4	47	16
176	4	52	16
209	5	54	16
240	5	57	16
269	5	57	16
342	5	57	16

Figure 18. Deformation variation of the roadway with roadway excavating.

(2)　Stress Monitoring of Bolt and Cable

Table 5 and Figure 19 allow for the conclusion that the stresses on the bolts and cables were small and showed little change during the roadway excavation. The stresses on the roof bolt, right rib bolt, and roof cable remained unchanged with tightening forces of 48 kN, 39 kN, and 68 kN, respectively. Moreover, the stress on the left rib bolt increased by 8 kN, but the value was still small. This indicates that the roadway was in a low stress state and shows the support of the bolt plus the cable is more effective.
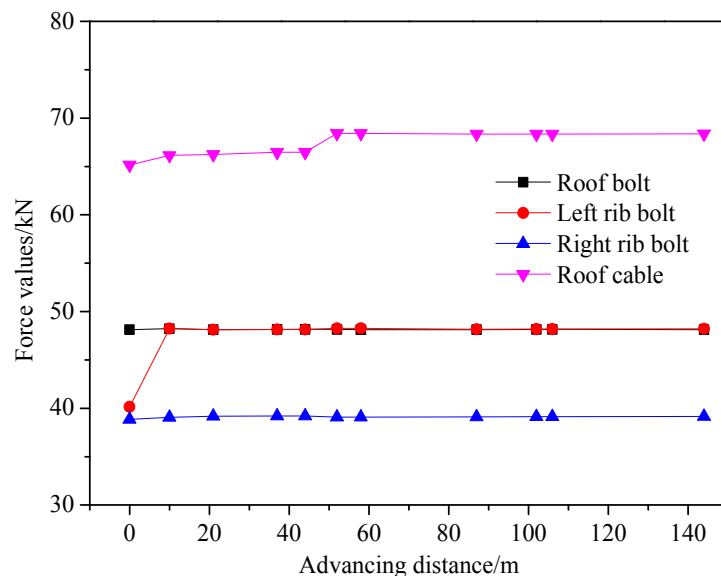

Figure 19. Stress variation of the bolt and cable with the roadway excavation.

Table 5. Stress variation of the bolt and cable with the roadway excavation.

Excavating Distance/m	Roof Bolt/kN	Right Rib Bolt/kN	Left Rib Bolt/kN	Roof Cable/kN
1.5	48	39	40	65
9	48	39	48	66
40.5	48	39	48	66
49.5	48	39	48	66
57	48	39	48	66
72.5	48	39	48	68
86	48	39	48	68
101.5	48	39	48	68
105.3	48	39	48	68
143	48	39	48	68
176	48	39	48	68
209	48	39	48	68
240	48	39	48	68
269	48	39	48	68
342	48	39	48	68

(3) Endoscopy Results of Roof Failure

A drill hole was set up on the roadway roof and the rock failure with different depths depicted by an electronic drilling peep instrument, as shown in Figure 20.

Figure 20 shows that there was no severe damage to the roof except that a vertical crack at the depth of 2 m occurred. The drill hole was basically intact, and there was no bed separation observed in the roof rocks. This shows that the surrounding rocks of the roadway formed an effective load-bearing structure with the support of the bolt and cable, and the support was better.
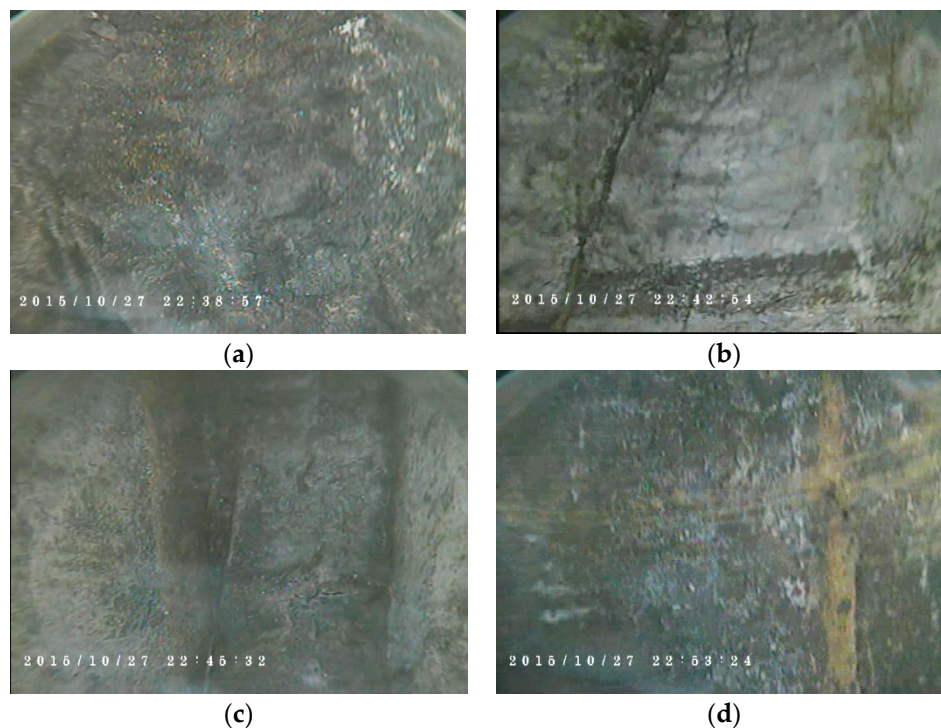

Figure 20. Rock failure with different depths depicted by electronic drilling peep instrument. (**a**) Drill hole depth of 1 m; (**b**) Drill hole depth of 2 m; (**c**) Drill hole depth of 3.5 m; and (**d**) Drill hole depth of 4.5 m.

(4)　Results of Roof Bed Separation

Two monitoring points were set up at the roadway roof with different heights—2.4 m and 6.0 m—to study the bed separation of the roof, as shown in Table 6 and Figure 21.

Table 6. Variation of the roof bed separation with the roadway excavation.

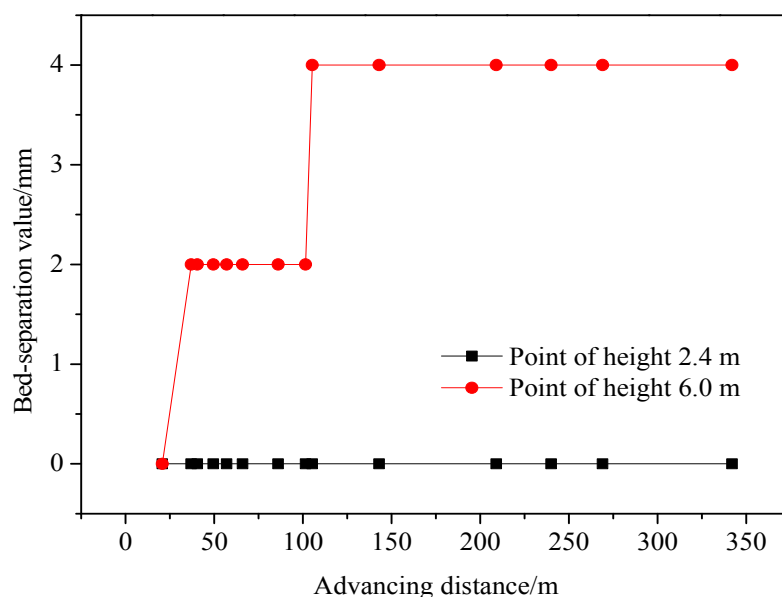| Excavation Distance/m	Roof Bed Separation Values/mm	
	Monitoring Point of Height 2.4 m	Monitoring Point of Height 6.0 m
20.7	0	0
37	0	2
40.5	0	2
49.5	0	2
57	0	2
66	0	2
86	0	2
101.5	0	2
105.3	0	4
143	0	4
209	0	4
240	0	4
269	0	4
342	0	4

Figure 21. Rock failure with different depths depicted by electronic drilling peep instrument.

Regarding the roadway excavation, the maximum bed separation values of the two monitoring points on the roadway using the bolt and cable support were insignificant at only 0 mm and 4 mm, respectively. This indicates that bed separation basically did not occur in the roof using this support scheme and further shows that a bolt and cable fixture had high efficiency for initial support, laying a good foundation for maintaining the long-term stability of the roadway.

5.2.2. Observation with Working Face Mining

During mining, a section of the roadway with the distance from the open-off cut of 50 m was selected as a monitoring station to survey the roof subsidence and two ribs' convergence by the method of cross-cloth point.

Figure 22, with the mining area approaching the surveyed section, shows the two ribs' convergence rose exponentially and tended to be stable. However, the value with the distance of 10 m was only 5 mm, and it was in a low level. This indicates that the deformation of the two ribs was affected by the mining activities and shows certain periodicity; moreover, it also shows that the support effect of the bolt and cable applied to the roadway was noteworthy.
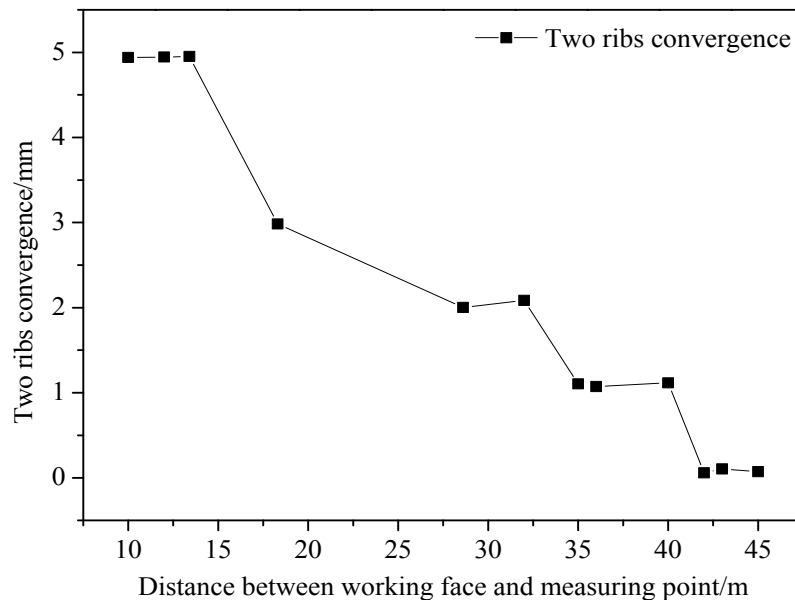

Figure 22. Variation curve of the two ribs' convergence for the roadway section.

Figure 23 shows that the roof subsidence rose slowly as the mining area approached the surveyed section, while the distance of 10 m had a value of 14 mm. This indicates that the abutment stress had no abrupt change, and the roof moved smoothly; moreover, it also shows that the support of the bolt and cable applied to the roadway was better and significant.
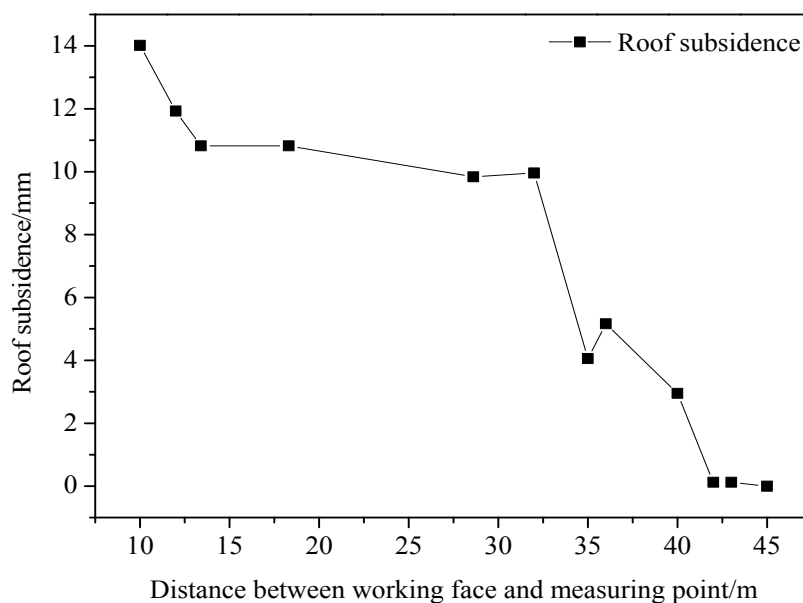

Figure 23. Variation curve of the roof subsidence for the roadway section.

Comparing the prior numerical simulation results to the support and field observation results after installing anchors, the field observation results of the roof subsidence and two rib convergence during the roadway excavation process (9 mm and 16 mm shown in Figure 18 and Table 4) had more significance than that of just the numerical simulation results (180 mm and 115 mm shown in Figure 4). The stresses of the bolts and cables were small with little variation, as shown in Figure 19; it was very close to the installation stress at the initial stage of excavation. The stress of the roof cable rose to 68 kN, which was close to the installation stress of 80–100 kN, for example. Moreover, Figure 21 and Table 6 show the maximum roof bed separation value was only 4 mm, which indicates that bed separation basically does not occur in the roof affected by this support scheme. Thus, when a scheme of bolt and cable support was applied to the roadway of Panel 11-101 in the Tuanbai coal mine, the roadway deformation was small, the bolt/cable stress was low, and the roof fracture was rarely observed. Hence, it can be concluded that the support scheme is reliable and effective to control the deformation of a roadway, thereby ensuring the safety of the roadway support. Moreover, the results of the field observation verify the aforementioned numerical simulation results and deserve further promotion and application.

6. Conclusions

Based on the technical problem of support for a water-dripping roadway below a contiguous seam goaf in the Tuanbai coal mine, this study on the deformation and control countermeasures of the surrounding rocks for water dripping on a roadway was carried out in detail by means of numerical simulation, theoretical analysis, and field observation. The main study contents and the conclusions are obtained as follows:

- The deformation of the water-dripping roadway was noticeable and showed marked effect over time, particularly during the roadway excavation and mining. It presented significant stage characteristics as follows: during the initial stage of roadway excavation, the roadway deformation rose sharply, and then it varied slightly in the middle and late stages of the roadway excavation, at which point the deformation of the roof and two ribs increased, while the floor heave decreased. During the stage of mining, the deformation rose again while affected by mining activities; however, the deformation of the roof and two ribs showed ladder-shaped growth, while that of the floor heave presented a significant displacement oscillation characteristic.

- Based on the large deformation of the surrounding rocks by the dripping water onto the roadway, the mechanical models of surrounding rocks with bolt supports was established; the effect of the bolt anchorage length and water-dripping erosion on the strength of rocks was studied. The authors found that there was an optimal value for the anchor length support for the roadway, and the support effect increased noticeably with an increase in length following the point where the length was less than the value. It was not obvious once the length exceeded the value; moreover, the effect weakened significantly as the water-dripping erosion factor on the bolt rose. Hence, a bolt with a reasonable anchor length and waterproof fixative agent can help to exert the needed support for the surrounding rocks of the water-dripping roadway.

- According to the above conclusions, a combined support scheme of bolt and cable was recommended, and two important technical parameters of bolt support (line spacing and tightening force) were studied in detail. Finally, the reasonable and optimized parameters of spacing and the tightening force of bolts were found to be 0.7–0.9 m and exceeding 40 kN, respectively.

- Combined with the above study results and the actual conditions at the Tuanbai coal mine, feasible measures for bolt and cable support were proposed. A field case regarding the deformation of the surrounding rocks, monitoring of anchor stress, endoscopy results of roof failure, and roof bed-separation monitoring were used to verify the logic of the scheme.

The study results can serve as a reference regarding supports for a roadway with water dripping onto it under similar conditions.

References

1. Wang, J.C.; Liu, F.; Wang, L. Sustainable coal mining and mining sciences. *J. China Coal Soc.* **2016**, *41*, 2651–2660.

2. Sui, W.H.; Hang, Y.; Ma, L.X.; Wu, Z.Y.; Zhou, Y.J.; Long, G.Q.; Wei, L.B. Interactions of overburden failure zones due to multiple-seam mining using longwall caving. *Bull. Eng. Geol. Environ.* **2015**, *74*, 1019–1035. [CrossRef]

3. Gu, R.; Ozbay, U. Numerical investigation of unstable rock failure in underground mining condition. *Comput. Geotech.* **2015**, *63*, 171–182. [CrossRef]

4. Coggan, J.; Gao, F.Q.; Stead, D.; Eimo, D. Numerical modelling of the effects of weak immediate roof lithology on coal mine roadway stability. *Int. J. Coal Geol.* **2012**, *90–91*, 100–109. [CrossRef]

5. Liang, Y. Scientific conception of precision coal mining. *J. China Coal Soc.* **2017**, *42*, 1–7.

6. Li, H.; Lin, B.Q.; Hong, Y.D.; Gao, Y.B.; Yang, W.; Liu, T.; Wang, R.; Huang, Z.B. Effects of in-situ stress on the stability of a roadway excavated through a coal seam. *Int. J. Min. Sci. Technol.* **2017**, *27*, 917–927. [CrossRef]

7. Wang, P.; Jiang, L.S.; Jiang, J.Q.; Zheng, P.Q.; Li, W. Strata Behaviors and Rock Burst–Inducing Mechanism under the Coupling Effect of a Hard, Thick Stratum and a Normal Fault. *Int. J. Geomech.* **2018**, *18*, 04017135. [CrossRef]

8. Zhang, N.C. *Stress Redistribution Law of Floor Strata under Chain Pillar and Its Application in Multi-Seam Mining*; China University of Mining and Technology: Xuzhou, China, 2016.

9. Yan, H.; Weng, M.Y.; Feng, R.M.; Li, W.K. Layout and support design of a coal roadway in ultra-close multiple-seams. *J. Cent. South Univ.* **2015**, *22*, 4385–4395. [CrossRef]

10. Liu, R.C.; Li, B.; Jiang, Y.J. A fractal model based on a new governing equation of fluid flow in fractures for characterizing hydraulic properties of rock fracture networks. *Comput. Geotech.* **2016**, *75*, 57–68. [CrossRef]

11. Liu, R.C.; Li, B.; Jiang, Y.J. Critical hydraulic gradient for nonlinear flow through rock fracture networks: The roles of aperture, surface roughness, and number of intersections. *Adv. Water Resour.* **2016**, *88*, 53–65. [CrossRef]

12. Hao, S.Z. *The Bolt Support Mechanism Study of Wake Rock Burst Roadway*; Chongqing University: Chongqing, China, 2016.

13. Li, B. *Research on the Layout Optimization and the Support System in Close Coal Seams*; China University of Mining and Technology: Beijing, China, 2012.

14. Zhao, Y.F. Numerical analysis on roof raining affected to surrounding rock deformation of mine gateway. *Coal Sci. Technol.* **2012**, *40*, 27–34.

15. Yang, R.S.; Li, Y.L.; Guo, D.M.; Yao, L.; Yang, T.M.; Li, T.T. Failure mechanism and control technology of water-immersed roadway in high-stress and soft rock in a deep mine. *Int. J. Min. Sci. Technol.* **2017**, *27*, 245–252. [CrossRef]

16. Yang, Z.W. On influence factors of stability of roadway under many gobs in ultra-close coal seams and supporting countermeasures. *China Coal* **2014**, *40*, 60–64.

17. Wu, A.M.; Zuo, J.P. Reasearch on the effects of multi-mining on activity law of rock strata in close coal seams. *J. Hunan Univ. Sci. Technol. (Nat. Sci. Ed.)* **2009**, *24*, 1–6.

18. Dunning, J.; Douglas, B.; Miller, M.; McDonald, S. The role of the chemical environment in frictional Deformation: Stress corrosion cracking and comminution. *Pure Appl. Geophys.* **1994**, *43*, 151–178. [CrossRef]

19. Hawkins, A.B.; Mcconnell, B.J. Sensitivity of sandstone strength and deformability to changes in moisture content. *Q. J. Eng. Geol. Hydrogeol.* **1992**, *25*, 115–130. [CrossRef]

20. Chugh, Y.P.; Missavage, R.A. Effects of moisture on strata control in coal mines. *Eng. Geol.* **1981**, *17*, 241–255. [CrossRef]

21. Ren, W.F. *Theory Research of Stress Field Displacement Filed and Seepage Filed and Study in Grouting Waterproofing of High Water Pressure Tunnel*; Central South University: Changsha, China, 2013.

22. Zhang, Z.W.; Wu, J.N.; Fan, M.J.; Gao, F.Q.; Zhang, L.H. Research on Roadway Support Technology Under Goaf of Close Coal Seam. *Coal Eng.* **2015**, *47*, 37–40.

23. Jiang, L.S.; Wang, P.; Zhang, P.P.; Zheng, P.P.; Xu, B. Numerical analysis of the effects induced by normal faults and dip angles on rock bursts. *C. R. Mecanique* **2017**, *345*, 690–705. [CrossRef]

24. Itasca Consulting Group. *FLAC3D: Fast Lagrangian Analysis of Continua 3D User's Guide*; Itasca Consulting Group: Minneapolis, MI, USA, 2005.

25. Gao, F.Q.; Stead, D.; Kang, H.P.; Wu, Y.Z. Discrete element modelling of deformation and damage of a roadway driven along an unstable goaf—A case study. *Int. J. Coal Geol.* **2014**, *127*, 100–110. [CrossRef]

26. Wang, W.; Cheng, Y.P.; Wang, H.F.; Liu, H.Y.; Wang, L.; Li, W.; Jiang, J.Y. Fracture failure analysis of hard-thick sandstone roof and its controlling effect on gas emission in underground ultra-thick coal extraction. *Eng. Fail. Anal.* **2015**, *54*, 150–162. [CrossRef]

27. Li, S.C.; Wang, H.T.; Wang, Q.; Jiang, B.; Wang, F.Q.; Guo, N.B.; Liu, W.J.; Ren, Y.X. Failure mechanism of bolting support and high-strength bolt-grouting technology for deep and soft surrounding rock with high stress. *J. Cent. South Univ.* **2016**, *23*, 440–448. [CrossRef]

28. Cheng, L.; Zhang, Y.D.; Ji, M.; Zhang, K.; Zhang, M.L. Experimental studies on the effects of bolt parameters on the bearing characteristics of reinforced rock. *SpringerPlus* **2016**, *5*, 866. [CrossRef] [PubMed]

29. Lister, J.R.; Kerr, R.C. Fluid-mechanical models of crack propagation and their application to magma transport in Dykes. *J. Geophys. Res.* **1991**, *96*, 10049–10077. [CrossRef]